INFLUENCE OF CAVITATION ON TURBULENT SEPARATED FLOW

Takeo Kajishima
Department of Mechanical Engineering,
Osaka University
Yamadaoka, Suita, Osaka, 565-0871 Japan
kajisima@mech.eng.osaka-u.ac.jp

Takashi Ohta
Department of Mechanical Engineering,
Osaka University
ota@mech.eng.osaka-u.ac.jp

Hiroki Sakai
Graduate School of Engineering,
Osaka University
current affiliation: Sumitomo Metal Industries, Ltd.

Kie Okabayashi
Graduate School of Engineering,
Osaka University
oka-kie@fluid.mech.eng.osaka-u.ac.jp

ABSTRACT

Attention was focused on the interaction between vortex and cavitation as a basic study on modeling unsteady turbulent flows with cavitation. First, separated shear layer with cavitation were directly simulated. Cavitation caused by spanwise and streamwise vortices, which are typical features in high shear layer, was represented by a simple model. Experimentally observed tendencies in the location of vortex formation, the frequency of vortex shedding and the intensity of Reynolds stresses were reasonably reproduced. Influence of cavitation on a typical example of streamwise vortex was observed. It was found that the vorticity in the core of Burgers type vortex was significantly reduced. To establish a description of it, we used an artificially maintained Burgers vortex. As a result, an assumption of constant circulation along a closed circle expanding due to sudden development of cavity could represent the modification of the vortex.

INTRODUCTION

Flows in hydro-machineries are affected by various types of cavitation. Since 1990's, several methods have been proposed for the numerical simulation of flow fields including unsteady cavitation. Attached (sheet) cavitation and cloud (bubble) cavitation have been reasonably reproduced. However, the influence of turbulence has not been taken into account completely in previous simulations although most of cavitating flows are turbulent. This causes inaccuracy in predicting the cavitation inception because the local minimum of pressure is thought to be corresponding to the core of turbulence vortices. On the other hand, the effect of cavitation on turbulence has usually been omitted. Therefore, to establish the computational method for turbulent cavitating flows, the interaction between cavitation and turbulence vortices should be correctly modeled.

The aim of our study is to address the modeling strategies considering two questions. (1) How are fine-scale vortices in turbulence related to cavitation inception? (2) How does the cavitation modify turbulent vortices and turbulence statistics? Since both are interactive phenomena, they must be analyzed by two-way methodology.

One of typical and appropriate examples for our objective is the separated flow in the wake of a thin fence in a two-dimensional channel. Iyer and Cessio (2002) visualized various types of vortex cavitation and they reported the turbulence statistics in the wake region.

In the first half of this report, we show the results of the direct numerical simulation with cavitation model, which was developed by Okita and Kajishima (2002). Our result is compared with experimental observation by Iyer and Cessio (2002) qualitatively, because the flow configuration was simplified in our simulation. Then, we investigate the relationship between cavitation and vortical structure; namely, primary (spanwise) vortices and the secondary (streamwise) vortices.

In the second half, the interaction between a Burgers vortex and cavitation is directly simulated in an idealized situation. One reason is that streamwise vortices in a shear layer, simulated in the former part, has a profile of Burgers vortex. Moreover, the finest scale eddies in fully developed turbulence has been found to be Burgers type. A Burgers vortex in a uniform stream is given at the inlet cross section of the computational domain for this purpose. Reducing the cavitation number, the structure of vortex decaying by cavitation inception is analyzed. Then we give a phenomenological model that represents the vortical structure during this process.

OUTLINE OF COMPUTATION

The procedure including cavitation model and numerical method should fit in with the spatio-temporal scale of unsteady motion of vortices in the turbulent shear layer. In this study, we apply the method developed by Okita and Kajishima (2002), which is a modification of Chen and Heister (1995).

Hereafter, all variables are non-dimensionalized by a characteristic length H, velocity u_∞, and the liquid density $\rho_{L\infty}$ at sufficiently far position. The flow field is assumed to be isothermal. A low-Mach number assumption is applied considering the weak compressibility of liquid.

The governing equations are the conservation laws of mass and momentum of homogeneous mixture of liquid and cavity:

$$\frac{Df_L}{Dt} + f_L\left(M^2\frac{Dp}{Dt} + \frac{\partial u_i}{\partial x_i}\right) = 0 \tag{1}$$

$$\frac{\partial u_i}{\partial t} + u_j\frac{\partial u_i}{\partial x_j} = -\frac{1}{f_L}\frac{\partial p}{\partial x_i} + \frac{1}{Re}\frac{\partial^2 u_i}{\partial x_j \partial x_j} \tag{2}$$

where u_i is the velocity component, p the pressure, and f_L the volumetric fraction of liquid. A Mach number $M(= u_\infty/c,\ \ c$ the sound speed) is given uniformly in a computational domain.

Omitting the second-order derivative, viscous and surface tension terms in Rayleigh-Plesset equation derives

$$\frac{dR}{dt} = \sqrt{\frac{2(p_v - p)}{3\rho_L}} \tag{3}$$

for $p < p_v$, which represents the increase rate of bubble radius R. Through an expansion of square-root, we obtain

$$\frac{df_L}{dt} = \frac{1-f_L}{\rho_L R}(p - p_v). \tag{4}$$

This equation simply means that cavitation region will expand under the condition of $p < p_v$, whereas it will contract in the region of $p > p_v$. It is similar to the model proposed by Chen and Heister (1995): $D\rho/Dt = C(p - p_v)$. An empirical constant C in their model seems to be related to the bubble diameter as supposed from Eq.(4). However, R can not be determined because bubble of varied size are included in the actual cavitating flow. Chen and Heister (1995) used very wide range of value for C: namely, 500, 5000 and 50000. It may related to the variation of R. Another problem of Eq.(4) in the actual computation is that the right hand side can not become negative when $f_L = 1$. Considering these problems, Okita and Kajishima (2002) used

$$\frac{Df_L}{Dt} = \Big[C_g(1-f_L) + C_l f_L\Big](p - p_v). \tag{5}$$

Two parameters, C_g and C_l, are to be determined from two viewpoints, which are comparison with experiment and numerical stability.

In the present study, Mach number is kept constant $M = 0.1$. The model constants are $C_g = 1000$ and $C_l = 1$ for $p < p_v$ (inception and growth of cavity) whereas $C_g = 100$ and $C_l = 1$ for $p > p_v$ (contraction and disappearance of cavity). They are same values used in Okita and Kajishima (2002), without any tuning particularly for the current problem.

The saturated vapor pressure p_v is given by

$$\sigma = \frac{p_\infty - p_v}{\frac{1}{2}\rho_L u_\infty^2} \tag{6}$$

corresponding to the cavitation number σ, where p_∞ and ρ_L is the pressure and liquid density at far distance.

The readers is referred to Okita and Kajishima (2002) for the detail of computational method.

CAVITATING FLOW IN UNSTEADY SHEAR LAYER

In the shear layer, large-scale spanwise vortices are generated due to the instability. In the stretched region between two neighboring vortices, streamwise (rib) vortices are caused by the secondary instability. Katz (1984), Katz and O'Hern (1986) and O'Hern (1990) pointed out cavitation takes place at the core of these vortices when the pressure become lower than the vapor pressure. Katz and O'Hern (1986) reported streamwise vortices contribute the cavitation inception.

The target of our computation is a separated shear layer including three dimensionality. The flow field is a simplified from that in the experiment by Iyer and Ceccio (2002). They produced a shear layer by putting a vertical plate with thin edge in the flow. Figure 1 shows our computational domain in a two-dimensional channel of the width H. The size of the domain is $H_x = 27.36H$ in the main stream direction and $H_z = 2H$ in the spanwise direction. At the distance $10H$ from the inlet, the plate of the height $0.225H$ is placed to create a shear layer.

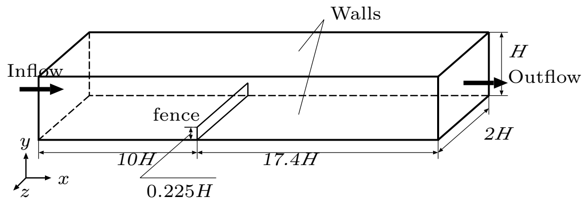

Figure 1: Overview of computational domain and boundary conditions for DNS of separated flow

Computational Condition

The numbers of grid points in each direction are 640 in the streamwise (x), 96 in the wall-normal (y), and 160 in the spanwise (z) directions. In x direction, 256 and 384 points are allocated respectively in upstream and downstream of the fence. Non-uniform distribution of grid is adopted in x direction for finer resolution in the vicinity of the fence.

We specify the boundary conditions separately from the experiment because they are not clear in Iyer and Ceccio (2002). At the inflow boundary, the parabolic profile without disturbance is given. At the outflow boundary, the convective boundary condition without reflection as described in Okita and Kajishima (2002) is used. The no-slip condition is applied at the wall and the periodicity is assumed in the spanwise direction.

Considering the experimental condition, 3 steps of cavitation number are dealt with: namely σ =0.50, 0.57 and ∞ (no cavitation).

Observation of Cavitating Turbulent Flow

Figures 2 and 3 shows instantaneous flow fields for single-phase and cavitating ($\sigma = 0.5$) flows. The mainstream is from left to right. The figure includes the domain downstream of the fence. The fence edge is marked by the dashed line. Vortical structure is indicated by the iso-surface of the second invariant (II) of velocity gradient tensor.

In these figures, primary roll-cell vortices and secondary streamwise vortices are observed. Former ones are not so clear because of the smaller II values. As shown in Figure 3, cavitation regions are corresponding to vortex cores. The cavitation is developing also in a streamwise vortex (the lowest part of the figure).

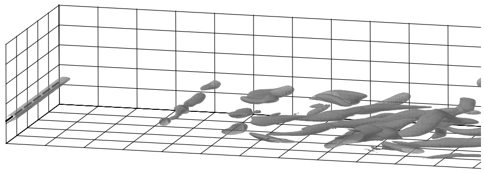

Figure 2: Overview of instantaneous flow field without cavitation (iso-surfaces of II = 10)

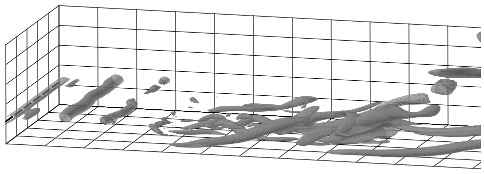

(a)Iso-surfaces of II = 10

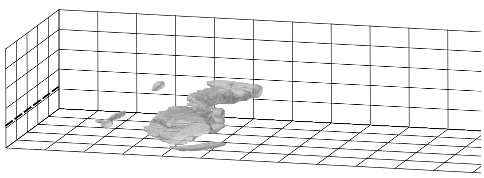

(b)Iso-surfaces of $f_L = 0.99$

Figure 3: Overview of instantaneous flow field with cavitation ($\sigma = 0.50$)

Figure 4 show the result of spectral analysis for the vertical component of velocity fluctuation. For single-phase flow, the primary peak is at around $f = 1.4$ and it is kept constant in downstream. In cavitating flow of σ =0.50, the fluctuation takes place in upstream side in comparison with single-phase case. The peak shifts to $f = 2.0$ at the origin. It however decreases while the spectrum is dispersed in downstream. Young and Holl (1966) and Belahadji, et al. (1995) measured the increase in the frequency of shed vortices in different kinds of experimental setup. Iyer and Ceccio (2002) suggested the influence of cavitation on the frequency but they did not show quantitative data.

The upstream shift of roll-cell formation affects the development of shear layer. As shown in Figure 5, the thickness of shear layer becomes larger in the case of cavitation. Correspondingly, the reattachment point shifts upstream in comparison with the single phase flow. These tendencies, as well as the change of turbulent stress profile, were also comfirmed experimentally by Iyer and Ceccio (2002).

Closeup of Streamwise Vortex with Cavitation

Figure 6 shows the time evolution of the profile of typical streamwise vortex under the condition of cavitation. For simplicity, the vortex core is selected as an instantaneous location where II takes the local maximum in the vortex. Abscissa of Figure 6 is z direction and its origin is the vortex core.

As shown in Figure 6(a), before and just after the cavitation inception (T =9.55 and 9.65), the profile of circumferential velocity is similar to that of Burgers vortex. In this situation, pressure reaches local minimum at the core of the vortex. Pressure once become lower than the vapor

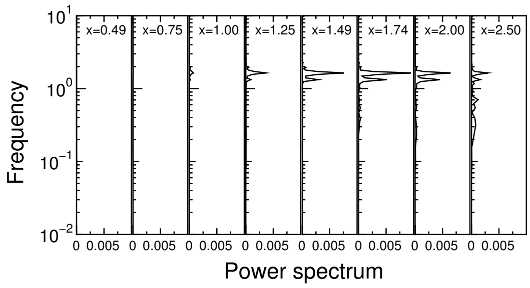

(a)Without cavitation

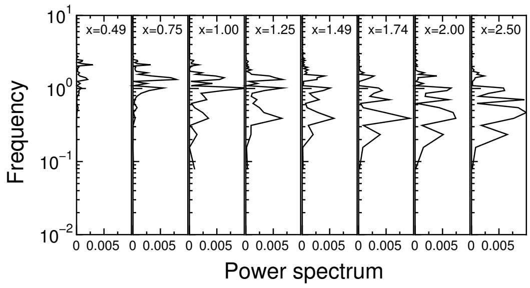

(b)With cavitation ($\sigma = 0.50$)

Figure 4: Influence of cavitation on frequency of spanwise vortex shedding

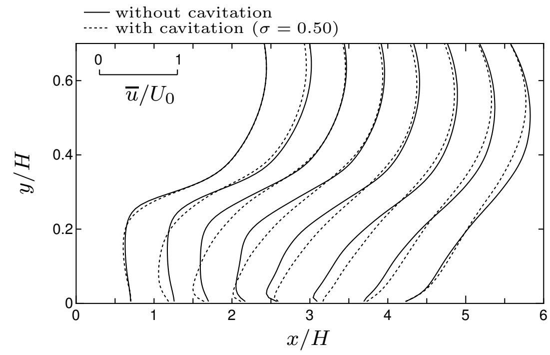

Figure 5: Profiles of streamwise mean velocity (development of shear layer thickness)

pressure and, consequently, cavitation grows till the pressure reaches to the vapor pressure, as shown in Figure 6(b). During the cavitation development, the circumferential velocity becomes smaller as shown in Figure 6(a). Accordingly, the axial vorticity become smaller in the core region as shown in Figure 6(c).

The above relation can be easily supposed as follows. The radial gradient of pressure decreases in the core. Also, the density of the gas-liquid mixture decreases due to the cavitation. Therefore, the vortical motion must become smaller to reduce the centrifugal force.

MODULATION OF ELEMENTARY VORTEX DUE TO CAVITATION

As shown in the previous section, the cavitation significantly affect the development of Burgers-like vortices in high shear layer. The fine-scale eddies in the Kolmogorov scale have also Burgers type profile, which is known as an elementary vortex in turbulence, e.g., Tanahashi, et al. (1997). Thus the better understanding of relationship between the

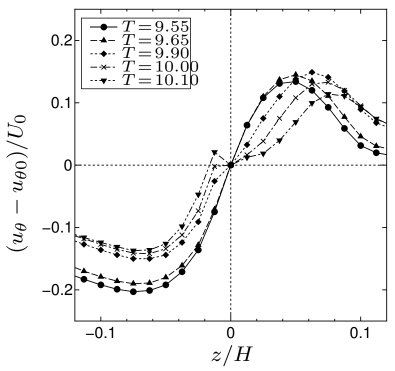

(a) circumferential velocity

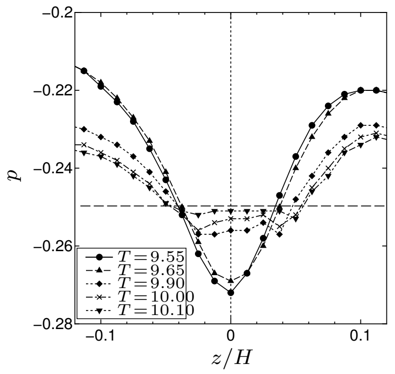

(b) pressure

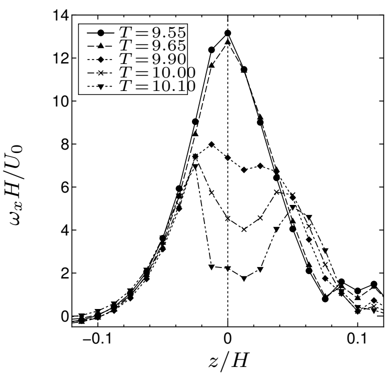

(c) axial component of vorticity

Figure 6: Evolution of a streamwise vortex under the cavitating condition σ =0.50

vortex and cavitation may address the modeling of cavitation inception in turbulence and, on the other hand, turbulence modulation by cavitation. However, it is not easy to observe the interaction in a tracking process of sample vortices in fully developed flow.

Thus we conduct a model simulation, in which a Burgers vortex is given in the inlet cross section and maintained in a uniform ambient flow. Then the cavitation number is reduced gradually to cause the cavitation at the vortex core. The systematic analysis for sensitivity to the cavitation number and the vortex strength will be reported elsewhere. Here we would like to propose a phenomenological model to describe the decay of vortex due to the cavitation.

Computational Condition

Figure 7 shows the outline of computational domain. The domain width D is selected for the length scale. The numbers of grid points in each direction are 64 in the streamwise (x), 32 in the cross sectional (y, z) directions. Computational cells are rectangular and distributed uniformly in the domain.

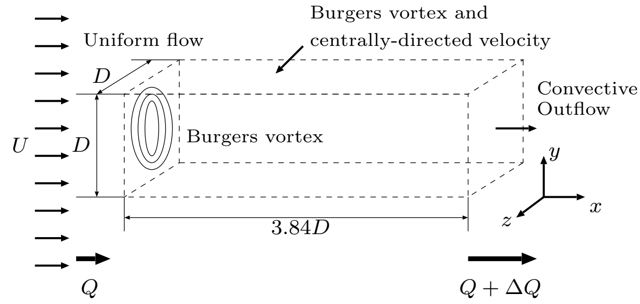

Figure 7: Overview of computational domain and boundary conditions for DNS of Burgers vortex

The inflow boundary condition for velocity is superpose of analytical solution of Burgers vortex and uniform flow U, which is used for the velocity scale. Burgers vortex approximates fine-scale vortices in turbulent flow (Tanahashi, et al., 1997), and its analytical solution is given by

$$v_\theta = \frac{\Gamma}{2\pi r}\left[1 - \exp\left(-\frac{\gamma}{4\nu}r^2\right)\right], \tag{7}$$

where Γ denotes the circulation, γ the stretching parameter and ν the kinetic viscosity. The velocity in the x direction at side boundaries is uniformly U. In addition, circumferential velocity of Burgers vortex at the inlet and the flow into the central axis are superposed as a side boundary condition. This boundary condition keeps and stretches the single vortex. Here, centrally-directed velocity causes the flow rate difference ΔQ between inflow and outflow. At the outflow boundary, convective boundary condition without reflection as described in Okita and Kajishima (2002) is used.

Computational conditions and parameters are given as follows: Reynolds number $Re(= DU/\nu_L) = 1 \times 10^3$. Time increment $\Delta t = 1 \times 10^{-3} D/U$; Cavitaion number $\sigma = 0.1$. Burgers vortex's parameters are given as: $\Gamma = 0.3$, $\gamma/\nu = 600$. ΔQ is 5% of Q, which is the flux given at the inflow. Parameters $\Gamma, \gamma/\nu$ and ΔQ are determined empirically in order to maintain a stable vortex.

Profiles of Velocity and Vorticity Influenced by Cavitation

Figure 8 shows instantaneous profiles of streamwise vortex and cavitation at two different moments. Figure 8(a) represents the vortex at the moment before cavity occurs, and Figure 8(b) includes the cavity region. Figure 8 suggests that vorticity is decreased by cavitation. Circumferential velocity v_θ and streamwise vorticity ω_x distributions are shown in Figure 9. The distribution indicated by the dotted line in each figure will be mentioned later. DNS results show that circumferential velocity and streamwise vorticity decrease when cavity expands. It is characteristic that circumferential velocity has milder gradient at vortex core. In addition, streamwise vorticity only at the vortex core decreases. These tendencies are observed also in DNS results of separated shear layer with cavitation (Figure 6(a), (c)).

Using Figure 10, we propose a possible model to represent the above-mentioned effect of cavitation. Before cavitating (Figure 10(a)), circumferential velocity along the circle of radius r is $v_\theta(r)$. In this situation, circulation Γ along this circumference is given by

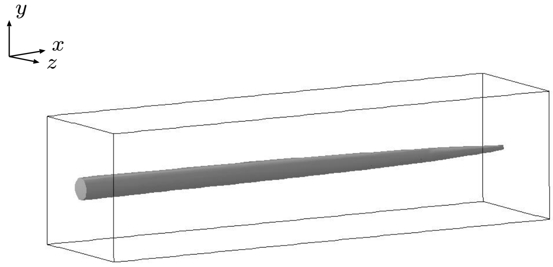

(a) Before cavitating

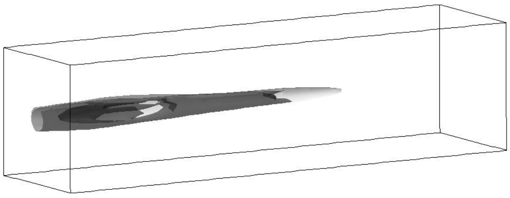

(b) After cavitation inception

Figure 8: Contours of vortex and cavitation indicated by $\omega_x = 4.85$ (dark gray) and $f_L = 0.9$ (light gray) isosurface

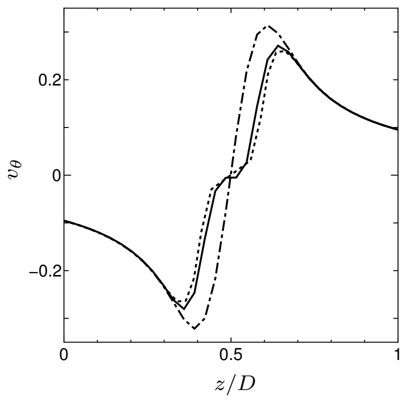

(a) Circumferential velocity

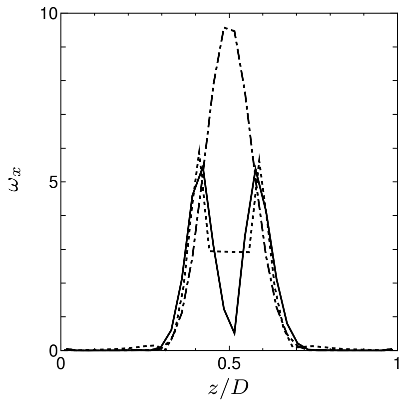

(b) Streamwise vorticity

Figure 9: Distribution shift by cavitation (In each figure, dashed-dotted line denotes DNS result before cavitating, solid line DNS result when cavitating and dotted line the result by the model)

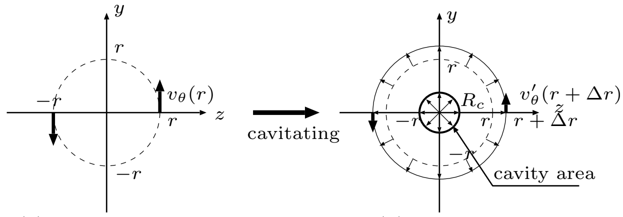

(a) Before cavitating

(b) Cavitating

Figure 10: Model for circumferential velocity prediction

$$\Gamma = 2\pi r v_\theta(r). \tag{8}$$

Expanding cavity pushes out the liquid (Figure 10(b)). Suppose the cavity displaces the liquid axsymmetrically in the radial direction. Liquid on circumference of radius r is also pushed out to radius $r + \Delta r$. The displacement is derived as $\Delta r = \sqrt{r^2 + {R_c}^2} - r$, where R_c is the equivalent radius of vortex cavity. The circumferential velocity becomes $v'_\theta(r + \Delta r)$. The circulation Γ' along the circumference of radius $r + \Delta r$ is given by

$$\Gamma' = 2\pi(r + \Delta r)v'_\theta(r + \Delta r). \tag{9}$$

If the circulation is conserved, during rapid cavity expansion, $v'_\theta(r + \Delta r)$ is given by

$$v'_\theta(r + \Delta r) = \frac{r}{r + \Delta r} v_\theta(r). \tag{10}$$

Circumferential velocity when cavitating is calculated based on this model. Here, R_c and v_θ are determined based on the analysis of DNS results. The dotted line in Figure 9(a) is v'_θ profile estimated by Eq. 10. Velocity by the model and DNS results coincide in maximum velocity and mild gradient at the vortex core. The model therefore is sufficient as a precondition to lead the velocity distribution shift.

The streamwise vorticity, which is determined by the model, is indicated in Figure 9(b) by the dotted line. It should be noted that the maximum value and its location of vorticity by the model agrees with DNS results. Therefore, vorticity distribution shift is successfully estimated by the model.

Prediction of Vortex Modification

In the previous section, we need R_c directly read from DNS results in order to calculate model-based velocity. In this section, we consider the method to estimate R_c. Cavity area $A_c(= \pi R_c^2)$ is introduced for the purpose of prediction of vortex modification without conducting fine-scale DNS. In this calculation, cavity is represented by liquid volumetric fraction f_L, and gas-liquid interface is not defined. Thus we suggest two method to calculate A_c as follows:

Method P_1: Assuming that the liquid on the circumference of radius r is pushed out by the cavity which used to be within the circumference, we define A_c as the area integration of gas volumetric fraction $1 - f_L$ within circumference of radius r. Thus, A_c depends on radius r.

Method P_2: Assuming that all cavity within the y-z cross-section is concentrated at the vortex core, we define A_c as the area integration of gas volumetric fraction $1 - f_L$ within the y-z cross-section.

Predicted velocity by two methods are shown in Figure 11(a) with DNS result when cavitating. Basically, method P_1, which provides the source of cavity at the central axis,

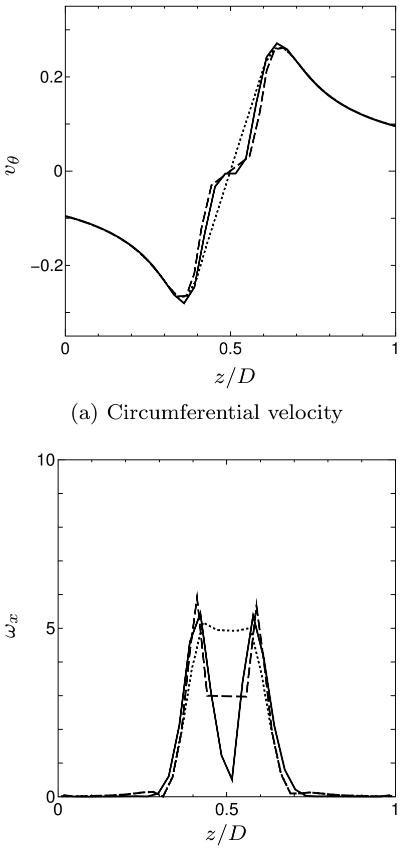

(a) Circumferential velocity

(b) Streamwise vorticity

Figure 11: Predicted circumferential velocity and streamwise vorticity (In each figure, solid line denotes DNS result, dotted line the predicted value by P_1 and dashed line the predicted value by P_2)

enables us to estimate actual cavity area which contributes to pushing out the liquid. Therefore, predicted velocity by P_1 and DNS result coincide except at the vortex core. At the vortex core, agreement between P_1 and DNS is not complete due to the radius r decreasing.

On the other hand, cavity area which contributes to pushing out the liquid cannot be estimated exactly by method P_2, but mild gradient observed in DNS result is almost expressed by the assumption of concentrating cavity at the vortex core.

As mentioned above, the method to decide R_c has not defined uniquely yet. However, both simple assumption could represent interaction phenomena between vortex and cavitation qualitatively. Figure 11(b) compares estimated streamwise vorticity to DNS result. Maximum vorticity of both prediction corresponds with DNS result.

CONCLUSION

The interaction between cavitation and artificially reproduced Burgers vortex is investigated by means of DNS. The DNS results suggest that circumferential velocity and streamwise vorticity of the vortex are decreased by cavity expansion. These interaction phenomena are qualitatively represented by our simple model, which is based on the assumption of constant circulation along a closed circle due to sudden cavity expansion. Moreover, structure similar to the Burgers vortex affected by cavitation was observed in our DNS of fully developed shear layer. If turbulence statistics are quantified, this model can provide the basic concept of cavitating turbulence model.

REFERENCES

Belahadji, B., Franc, J. P. and Michel, J. M., 1995, "Cavitation in the rotational structures of a turbulent wake", *J. Fluid Mech.*, Vol.287, pp.383-403.

Chen, Y., and Heister, S., 1995, "Two-phase modeling of cavitated flows", *Computer & Fluids*, Vol.24, No.7, pp.799-809.

Iyer, C. O. and Ceccio, S. L., 2002, "The influence of developed cavitation on the flow of a turbulent shear layer", *Phys. Fluids*, Vol.14, No.10, pp.3414-3431.

Katz, J., 1984, "Cavitation phenomena within regions of flow separation", *J. Fluid Mech.*, Vol.140, pp.397-436.

Katz, J. and O'Hern, T. J., 1986, "Cavitation in large scale shear flows", *J. Fluids Eng.*, Vol.108, pp.373-376.

O'Hern, T. J., 1990, "An experimental investigation of turbulent shear flow cavitation", *J. Fluid Mech.*, Vol.215, pp.365-391.

Okita, K. and Kajishima, T., 2002, "Three-dimensional computation of unsteady cavitating flow in a cascade", *Proc. 9th International Symposium on Transport Phenomena and Dynamic of Rotating Machinery*", Honolulu,(CD-ROM) No.FD-ABS-076.

Tanahashi, M., Miyauchi, J. and Ikeda, J., 1997, "Scaling law of coherent fine scale structure in homogeneous isotropic turbulence", *11th Symp. Turbulence Shear Flows*, No.4-17.

Young, J. O. and Holl, J. W., 1966, "Effects of cavitation on periodic wakes behind symmetric wedges" *J. Basic Eng.*, Vol.88, pp.163-176.